AGU PUBLICATIONS

JGR

Journal of Geophysical Research: Oceans

RESEARCH ARTICLE

10.1002/2014JC010571

Key Points:
- Expected future increase in Arctic river runoff intensifies ocean stratification
- Stronger vertical stratification leads to warming below surface mixed layer
- Changes in heat flux to the base of the ice and in ice thickness are small

Supporting Information:
- Table S1
- Supporting Information S1

Correspondence to:
A. Nummelin,
aleksi.nummelin@uib.no

Citation:
Nummelin, A., C. Li, and L. H. Smedsrud (2015), Response of Arctic Ocean stratification to changing river runoff in a column model, *J. Geophys. Res. Oceans*, *120*, 2655–2675, doi:10.1002/2014JC010571.

Received 7 NOV 2014
Accepted 25 FEB 2015
Accepted article online 02 MAR 2015
Published online 7 APR 2015

Response of Arctic Ocean stratification to changing river runoff in a column model

Aleksi Nummelin[1,2], Camille Li[1,2], and Lars H. Smedsrud[1,2,3]

[1]Geophysical Institute, University of Bergen, Bergen, Norway, [2]Bjerknes Centre for Climate Research, Bergen, Norway, [3]University Centre in Svalbard, Longyearbyen, Norway

Abstract A one-dimensional model of the atmosphere-ice-ocean column is used to study the effects of changing river runoff to the Arctic Ocean. River runoff is the largest contributor of freshwater to the Arctic and is expected to increase as the hydrological cycle accelerates due to global warming. The column model simulates the stratification of the Arctic Ocean reasonably well, capturing important features such as the fresh surface layer, the salty cold halocline, and the temperature maximum within the Atlantic Water layer. The model is run for 500 years with prescribed boundary conditions to reach steady state solutions. Increasing river runoff is found to strengthen the stratification and to produce a fresher and shallower surface mixed layer with warming (up to ~1°C for a doubling of present-day runoff) in the Atlantic Water layer below. An important consequence is that the effect of the larger vertical temperature gradient is able to balance that of the stronger stratification and yield a close to constant vertical heat flux toward the surface. As a result, the sea ice response is small, showing only slight increase (up to ~15 cm for a doubling of present-day runoff) in annual mean ice thickness. Limitations of the study include the idealized nature of the column model and uncertainties in the background vertical mixing within the Arctic Ocean.

1. Introduction

The Arctic Ocean is distinguished from the rest of the world's oceans by unique oceanographic conditions. At the surface is a cold, fresh surface mixed layer while deep below is a layer of warmer, saltier Atlantic Water (AW). In between is a halocline, a relatively thin layer of increasing salinity with depth. The resulting stratification is essential for the presence of Arctic sea ice, with the halocline protecting the cold surface layer from the heat stored in the AW layer below. One of the critical factors maintaining this stratification is freshwater supplied by continental river runoff, which increases as the hydrological cycle accelerates due to global warming [*Rawlins et al*., 2010]. The increase in runoff is already measurable, with a reported 9.8% increase in the 30 year period between 1977 and 2007 [*Overeem and Syvitski*, 2010]. While the projections for future changes are somewhat uncertain, a runoff sensitivity of 0.007 Sv/°C is estimated from observations [*Peterson et al*., 2002] and the multimodel CMIP5 ensemble predicts an increase of approximately 0.03 Sv (30%) by 2100 for the RCP8.5 scenario (see supporting information Figure S1). Understanding the effects of changing river runoff on the stratification, heat fluxes, and sea ice cover in the Arctic Ocean is the main goal of this study. To this end, we perform and analyze a series of sensitivity experiments using a one-dimensional atmosphere-ice-ocean column model.

A special feature of the stratification in the Arctic Ocean is the cold upper part of the halocline, which has higher salinities than the surface layer but temperatures still close to the freezing point. The cold upper halocline derives from waters formed on shallow shelves and in the Arctic proper during sea ice formation [*Rudels et al*., 1996; *Steele and Boyd*, 1998; *Rudels et al*., 2004]. This cold halocline effectively reduces the heat flux to the surface mixed layer from below because any mixing penetrating the halocline only entrains cold (close to freezing point temperature) water [*Steele and Boyd*, 1998].

The net effect of increased runoff on this system is not easy to predict. One might expect increased runoff to strengthen the stratification by freshening the surface. On the other hand, a fresher surface layer sets up a larger density contrast between the Arctic Ocean and the Nordic Seas. This could increase the surface outflow from the Arctic, leading to stronger entrainment of the warm AW below [*Stigebrandt*, 1981]. A fresher surface would also modify shelf water formation, a water mass that feeds into the cold halocline. These

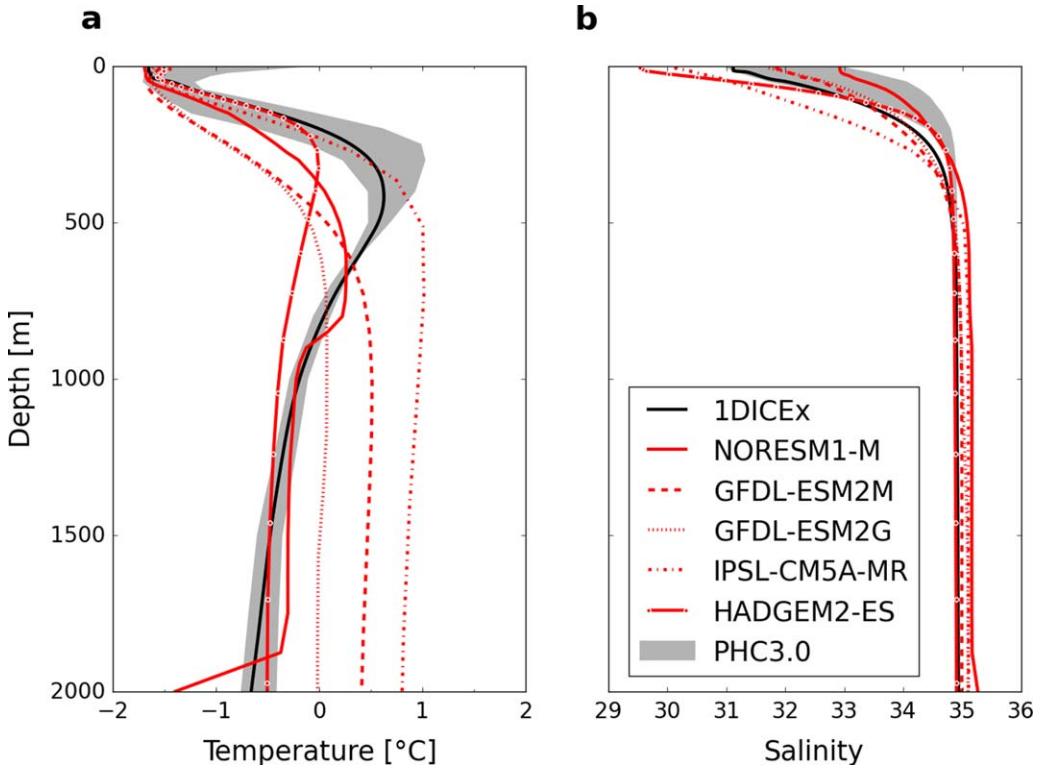

Figure 1. Observed and simulated (a) annual mean temperature and (b) salinity in the Arctic Ocean. Observed (PHC3.0 updated from *Steele et al*. [2001]) 25–75% quartile range is shown with gray shading. Results from the column model are shown in black. Selected climate model results for simulations of the 1970–2005 historical period are shown in red (Norwegian Earth System Model, NorESM [*Bentsen et al*., 2013], ESM2M and ESM2G [*Dunne et al*., 2012], HadGem2-ES [*Jones et al*., 2011], and IPSL-CM5A-MR [*Mignot et al*., 2013]), with profiles averaged over the Arctic Ocean (Barents Sea excluded).

various changes have different, and in some cases opposite, influences on the vertical heat flux toward the surface mixed layer and the base of the sea ice.

Climate models have trouble simulating the vertical structure of the upper Arctic Ocean (Figure 1), implying that they do not accurately represent some of the processes responsible for maintaining the stratification. Particularly difficult is capturing the strength of the halocline, as well as the depth and structure of the AW layer. The halocline and AW layer extend over a broader depth range in the models than in observations, are generally too weak and in most cases too deep (Figure 1). These features are crucial for a realistic response to perturbations in freshwater balance because they help set the vertical fluxes of heat among the ocean, ice, and atmosphere. This study uses an idealized one-dimensional coupled atmosphere-ice-ocean column model, motivated by the fact that the model is able to simulate these stratification features relatively well (Figure 1). The column model has a reduced set of variables and is computationally efficient, allowing us to perform many sensitivity experiments and to derive nearly steady state solutions. Furthermore, it is possible to separate forcings and responses and better interpret mechanisms that include complicated and contradicting feedbacks.

The original version of the column model used here was first presented by *Björk* [1989], and different versions have since been developed and used [e.g., *Björk and Söderkvist*, 2002; *Smedsrud et al*., 2008; *Linders and Björk*, 2013]. The model simulates a horizontally averaged vertical atmosphere-ice-ocean column. Originally, the model domain extended from the top of the atmosphere to the core of the AW layer at 300 m depth, where temperature and salinity were fixed to mean AW properties. In this study, we extend the model by expanding the model domain down to 2000 m and including a parameterization to compensate the heat loss due to upwelling from the AW layer (i.e., a prescribed heat convergence via Atlantic inflow with given T/S properties). The extended model allows the AW layer to respond dynamically to changes in river runoff and plays an active role in determining the resulting stratification.

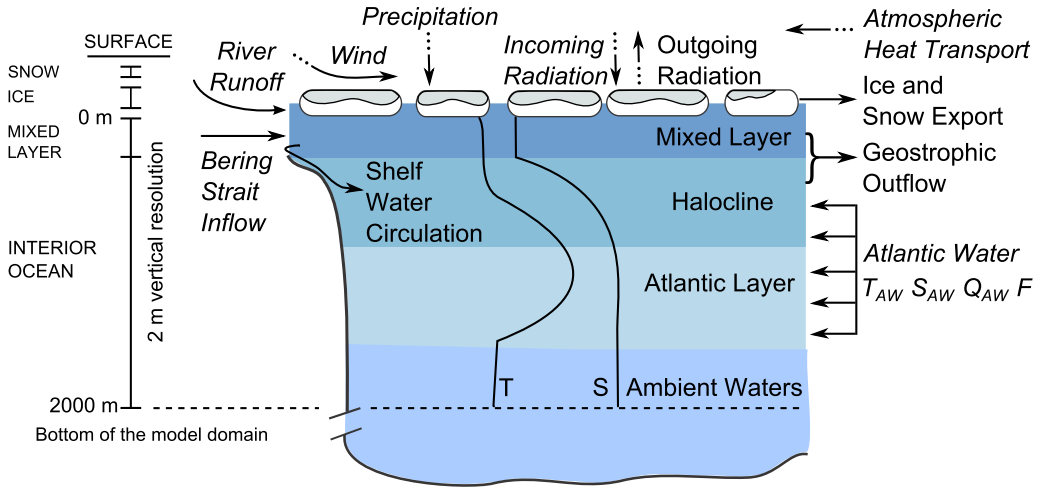

Figure 2. Sketch of the 1DICEx Arctic atmosphere-ice-ocean column model setup. The components of the model are indicated at the far left, and the cartoon shows the model forcings, simulated processes and resulting vertical stratification. See details and full list of abbreviations in the appendices.

The paper is structured as follows: we describe and evaluate the modified one-dimensional atmosphere-ice-ocean column model in section 2, present the results of the runoff experiments in section 3, and discuss the context and limitations of the study in section 4. Some conclusions on the effects of increased runoff on Arctic Ocean stratification and sea ice are presented in section 5. The model is described in more detail in Appendix A, a list of symbols is included in Appendix B, and the climatological forcing is given in Appendix C.

2. Extended 1DICE (1DICEx) Model

In this study, we use a version of the one-dimensional Arctic column model, 1DICE, which derives from the work of *Björk and Söderkvist* [2002] and *Björk* [1997, 1992, 1989]. Figure 2 shows a sketch of the setup used in this study. A more detailed description of the model including the extensions made in this study can be found in Appendix A.

The column model is set up to represent mean conditions in the Arctic Ocean following *Björk and Söderkvist* [2002]. The main forcings comprise climatological monthly mean values of atmospheric heat transport and downward shortwave radiation. The freshwater budget includes prescribed precipitation, river runoff, and transport from the Pacific Ocean through Bering Strait. There is an additional parameterized flow of brine-enriched water from the Arctic shelves to the deep Arctic basin. The surface outflow in the column is geostrophic and depends on the density gradient between the Arctic column and the Atlantic (the Atlantic is not explicitly included in 1DICEx, but prescribed AW properties are used). 1DICE includes a thermodynamic sea ice model with a ridging parameterization and up to 42 ice thickness classes. Sea ice export is driven by prescribed divergence based on measured values in the Fram Strait and the geostrophic surface outflow (Figure 2). The gray body atmospheric component of the model solves for atmospheric temperatures from prescribed atmospheric heat transport and solar radiation and calculated surface fluxes.

The present-day scenario uses a river runoff of 0.082 Sv [following *Björk and Söderkvist*, 2002], a value which is very close to the 0.088 Sv reported by *Lammers et al.* [2001] for the Arctic Ocean excluding the Barents Sea. The values for our runoff experiments are scaled from the climatology used by *Björk and Söderkvist* [2002], so we change the annual mean and monthly runoff, but preserve the seasonality of the forcing (see Appendix C for values of present-day scenario).

The main modification made for this study is the inclusion of an interactive AW layer in the column. This allows the temperature, salinity, and stratification of the column to adjust as we vary runoff. In the following sections, we discuss some of the assumptions related to the addition of the interactive AW layer and evaluate the performance of the extended 1DICEx model.

2.1. Interactive AW Layer

The bottom of the original model domain was set at 300 m. This bottom boundary was assumed to be the core of the AW layer, and temperature and salinity were fixed to constant "AW" values here. We have

extended the ocean column down to 2000 m to allow for an interactive AW layer, a modification that requires the addition of a heating term within the AW layer to compensate the surface heat loss and outflow. Physically, this can be seen as a parameterization for the heat and salt transported into the Arctic by the Atlantic inflow. Practically, it is implemented by requiring a fixed amount of AW heat transport at each time step and solving for the associated salt transport based on fixed AW *T/S* properties, which can largely be based on observations (see Appendix A and section 2.2).

In nature, variations in both volume transport and AW temperature can alter heat transport of the Atlantic inflow over a range of time scales. In the idealized approach used here, we set the temperature T_{AW} and salinity S_{AW} of the Atlantic inflow, as well as the heat supply H_{AW} needed to compensate the surface heat loss and outflow, to constants. The inflowing AW enters and adjusts with the column to form the AW layer. This approach allows us to isolate the mechanisms for Arctic Ocean changes related to variability in runoff from the mechanisms related to variability in properties of the inflowing AW. While this approach simplifies the analysis of the results, it carries certain implications.

First, in order to have heat transport from the Atlantic toward the Arctic, the heat content of the inflowing AW must be larger than the heat content in the Arctic column, i.e., $(\rho_{AW}T_{AW}) > (\rho T)$, where ρ_{AW} and T_{AW} are the (constant) density and temperature of the inflowing AW and ρ and T are the (prognostic) density and temperature of the column. In essence, the AW inflow needs to be warm enough to provide the required heat to the column. The salt transport into the column is a function of the heat transport and the AW inflow salinity (S_{AW}). S_{AW} cannot greatly exceed the salinity below the halocline, otherwise an unrealistic intermediate high salinity layer will form; it cannot be too low either, otherwise the halocline will be eroded.

Second, we must make certain decisions about the character of the AW inflow in the extended model. The inflow enters the column as a 500 m thick layer below the surface mixed layer ($Z_{AW} = 500$ m). The model physics then create the halocline and the AW layer in the interior ocean component (Figure 2). The halocline forms in the upper part of the interior ocean, and the AW layer is the location of the temperature maximum. Note that while Z_{AW} is constant, the AW inflow moves up and down following the annual cycle of the mixed layer depth. We set the vertical distribution of the AW heat transport to be a simple, barotropic boxcar (tests with a parabolic distribution produced similar results). While T_{AW} and S_{AW} are fairly well constrained by observations, there are less constraints on the vertical diffusion coefficient κ, which should be regarded mostly as a tuning parameter.

2.2. Evaluation and Sensitivity of the Extended Model

In this section, we describe how we tune the extended model to produce simulated T/S profiles as close as possible to available observations. We do this by running the model using a range of AW inflow properties (T_{AW}, S_{AW}, H_{AW}) and vertical mixing coefficients (κ), and identifying the combination of values that yield an ocean heat content that is closest to equilibrium. The resulting fluxes are then discussed at the end of the section.

The robustness of the model to the optimal values is shown in Figure 3, in which simulated T/S profiles are plotted as a function of T_{AW}, S_{AW}, and κ for $H_{AW} = 1$ TW. The T/S profiles are quite similar for the ranges $T_{AW} = [1.5, 4.0]^{\circ}$C, $S_{AW} = [34.8, 35.1]$, and $\kappa = [3.0–5.0] \times 10^{-6}$ m^2 s^{-1}. However, differences are apparent for some parameter combinations, mostly due to emerging convection. Closer inspection reveals that low T_{AW} and/or high S_{AW} leads to too much salt transport into the column and the formation of an intermediate salinity maximum around 500 m. It is only at values of T_{AW} and S_{AW} outside a realistic range that this salinity maximum appears in the model, although a there is some evidence of a subtle salinity maximum in some parts of the Arctic Ocean [*Rudels et al.*, 1994]. On the other hand, low S_{AW} results in a cooler AW layer because the smaller density gradient allows for more mixing toward the surface. The vertical diffusion coefficient κ has a larger effect on the simulated T/S profiles than the AW properties. Higher diffusion brings more heat up from the warm AW layer to the surface, but the choice of κ is also affected by the value of the compensating heat flux H_{AW} (not shown). Reasonable T/S profiles can only be attained over a narrow range of H_{AW}, otherwise the column warms up extensively, so this sets a practical limit on κ.

Given limited observations, especially for κ, we used the stability of the column's heat content to finalize the optimal T_{AW}, S_{AW}, and κ values. Figure 4 shows the change in heat content over the last 100 years of the 500 year runs as a function of T_{AW} and S_{AW} for three different values of κ. An optimal solution is simply a

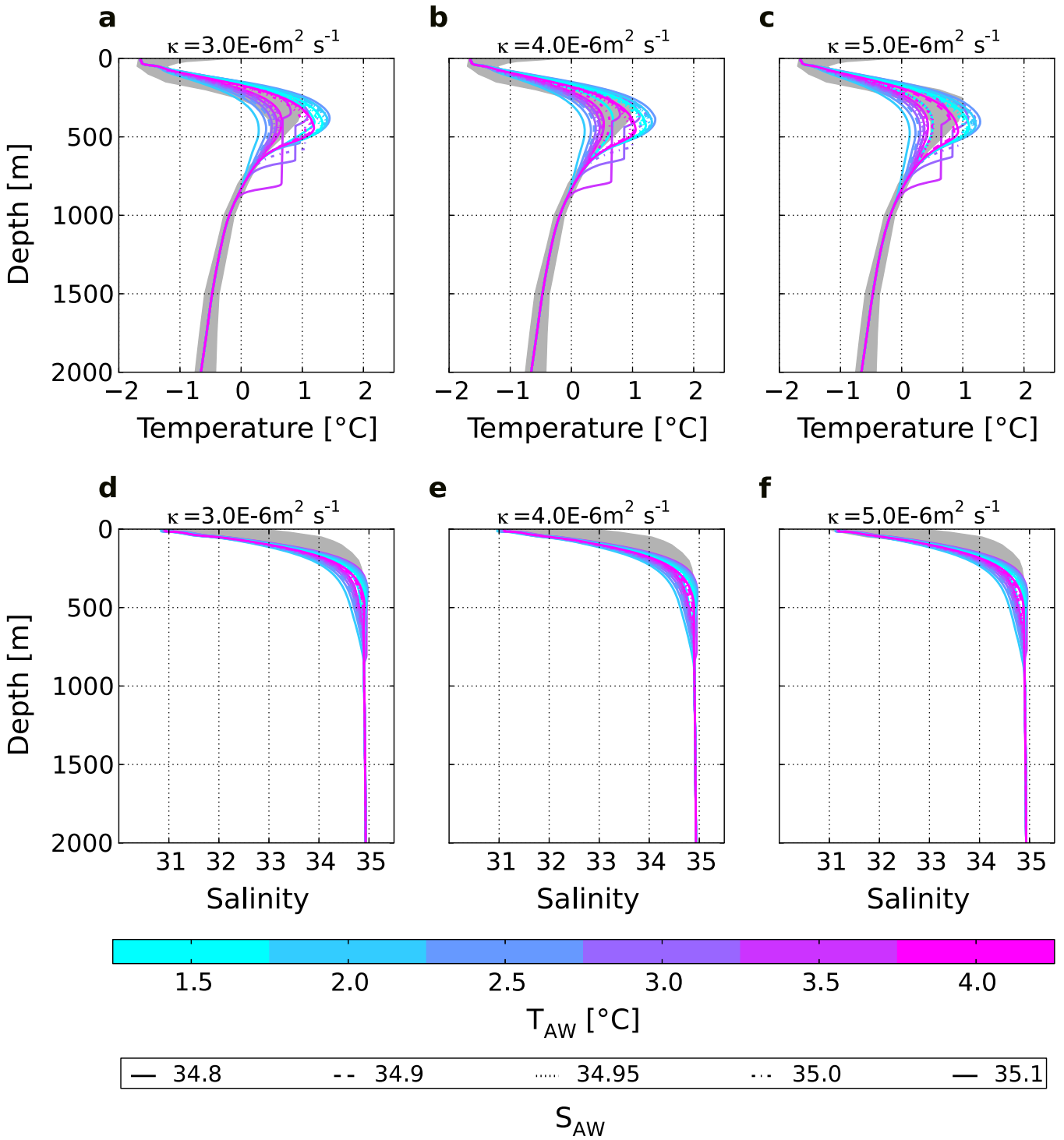

Figure 3. (top row) Simulated temperature (T) and (bottom row) salinity profiles (S) for three vertical diffusion coefficients (κ) and varying properties of inflowing Atlantic Water (T_{AW} indicated by different colors, S_{AW} indicated by different line types). Gray shading indicates the 25–75% quartile range calculated from observations (PHC3.0 updated from *Steele et al.* [2001]).

case where the change in the heat content $\frac{dE}{dt}$ is zero. It is possible to find such a solution by interpolating in T_{AW}-S_{AW}-κ space for the values where $\frac{dE}{dt}=0$. With the constraints provided by Figures 3 and 4, we arrive at values of $T_{AW}=3.5$°C and $S_{AW}=35.0$; a compensating heat flux of $H_{AW}=1$ TW by the AW inflow; and a vertical diffusion coefficient $\kappa=4.0\times10^{-6}$ m^2 s^{-1}. These values are comparable to the AW properties in the Fram Strait (PHC3.0 updated from *Steele et al.* [2001]), and κ values from the central Arctic Ocean [*Fer*, 2009].

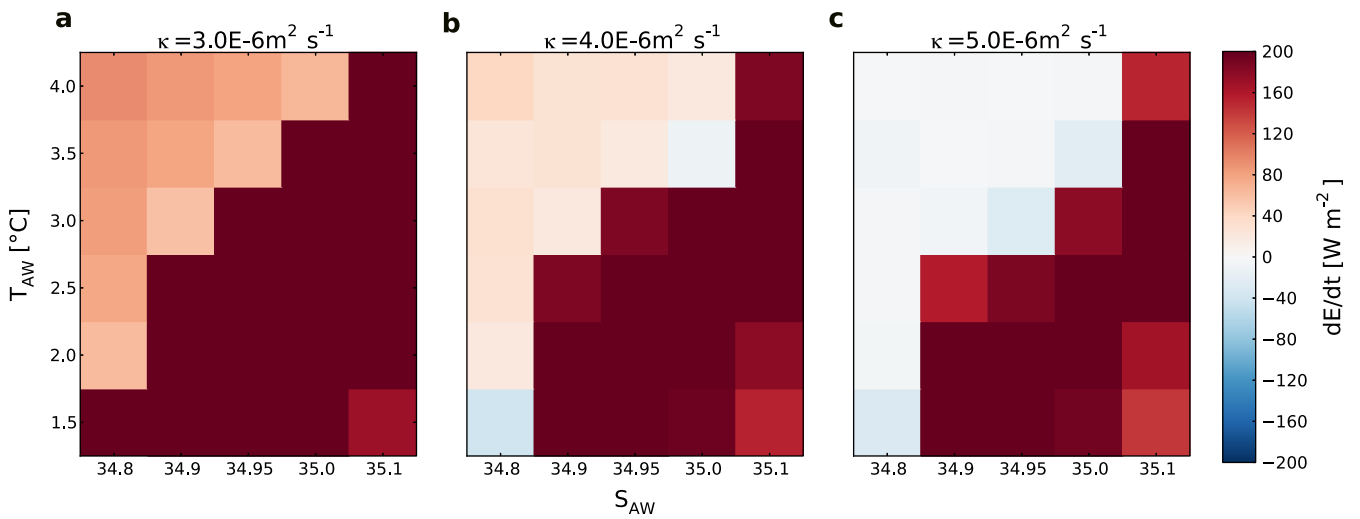

Figure 4. Simulated rate of change of internal energy $\left(\frac{dE}{dt}\right)$ over the last 100 years of each experiment for three vertical diffusion coefficients (κ) and varying properties of inflowing Atlantic Water (T_{AW}, S_{AW}).

As a consistency check, we examine the simulated volume and heat fluxes using the optimal values obtained above for the present-day runoff scenario. Details on how these fluxes are calculated appear in the introductory paragraph of this section and in Appendix A1. The main components of the freshwater budget in the present-day scenario are approximately 1.1 Sv of surface inflow (river runoff, Bering Strait inflow, and precipitation combined) balanced by approximately 1.2 Sv of geostrophic outflow in the upper part of the column. The outflow is of the same order of magnitude as observed (2–4 Sv) [*Marnela et al.*, 2013], although on the low side. The difference between the simulated and measured outflow could be due to several factors. First, we simulate a "steady state" Arctic Ocean. Observations covering a much shorter period should be expected to differ from such a long-term mean in any regard, but especially so for the Arctic today, which is undergoing rapid transition toward a warmer ocean and a thinner ice cover. Second, the simplified geostrophic outflow should not be expected to capture all aspects of reality, especially in complex regions like the Canadian Archipelago.

In addition to the main inflow and outflow terms, 1DICEx simulates 0.1 Sv of snow and ice export, which is a good match to the observed estimates of around 0.1 Sv [*Vinje*, 2001; *Spreen et al.*, 2009; *Schauer and Beszczynska-Möller*, 2009]. There is an additional 0.2 Sv of upwelling from the AW layer that balances the column volume fluxes. The associated $H_{AW} = 1$ TW heat supply converts to 0.13 W m^{-2} of heat flux toward the surface from below. This vertical heat flux also compares well with recent estimates of 0.1–0.2 W m^{-2} from the AW layer in the Canadian basin [*Lique et al.*, 2014].

2.3. Setup of River Runoff Experiments

In this study, we integrate 1DICEx over 500 years to obtain near-steady state solutions as a response to changing river runoff. The initial conditions for all runs are climatological conditions (PHC3.0 updated from *Steele et al.* [2001]), but river runoff is increased from just under one third (0.025 Sv) to just over 2 times (0.20 Sv) the present-day estimate of 0.082 Sv.

Figure 5 shows the adjustment of ocean temperature, salinity, and heat content for the various runoff scenarios over the 500 year simulation period. The mean temperature of the ocean column adjusts within the first few hundred years, although the highest and lowest runoff scenarios exhibit a small trend through the entire experiment. The column mean salinity equilibrates much more quickly, within a couple of decades, because it primarily reflects surface changes. With time, the heat content approaches steady state, and there is very little change over the last 200 years. Based on this analysis, we present results averaged over the last 100 years of each experiment, when most variables are close to steady state.

3. Results

To study the response of the Arctic Ocean to changes in river runoff, we run the 1DICEx column model with runoff values varying from 0.025 to 0.2 Sv. Reported present-day values are close to 0.1 Sv [*Peterson et al.*,

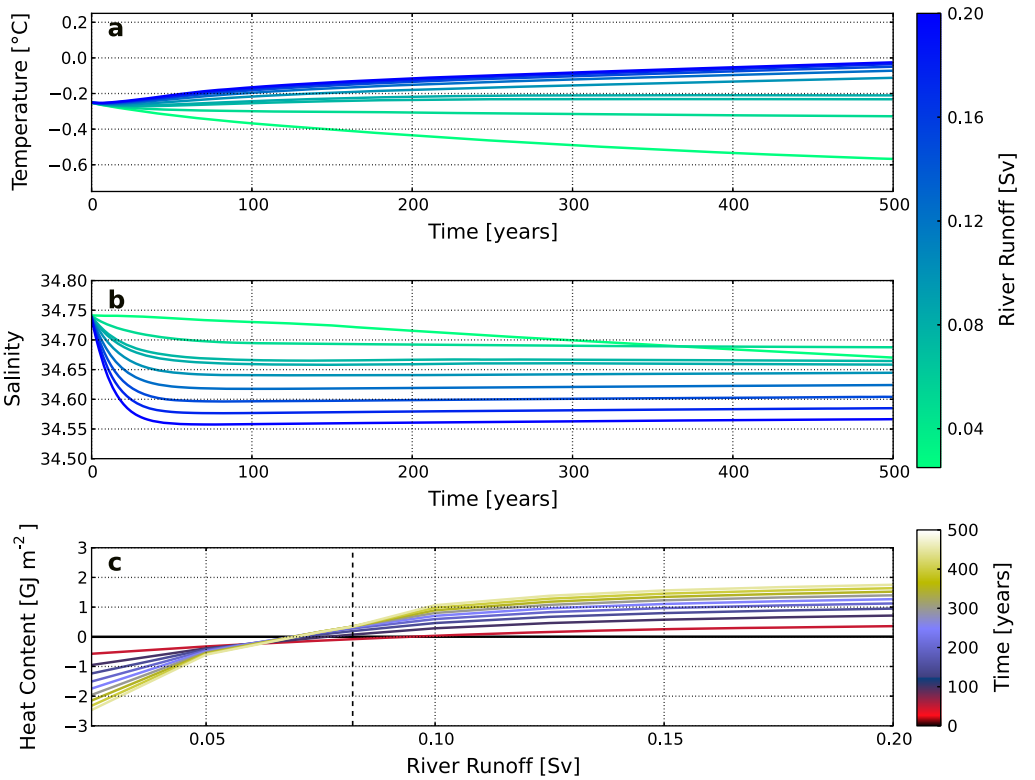

Figure 5. Transient response of 1DICEx model. Mass-weighted column-averaged (a) temperature and (b) salinity as a function of time (1 year running means); (c) column heat content anomaly referenced to initial conditions as a function of river runoff.

2002] for the pan-Arctic region and 0.088 Sv for the Arctic proper [*Lammers et al*., 2001], which is the domain of interest here. A 9.8% increase is reported for the period between 1977 and 2007 [*Overeem and Syvitski*, 2010], while the projections for future runoff changes are rather uncertain, e.g., sensitivity of 0.007 Sv/°C from observations [*Peterson et al*., 2002] and approximately 30% increase by 2100 in RCP8.5 for multi-model CMIP5 ensemble (supporting information Figure S1). The 0.025–0.2 Sv range of our experiments spans this uncertainty.

3.1. Ocean Response

The most obvious effect of increased river runoff is a freshening of the surface ML and the upper halocline (Figures 6a and 7). The annual mean surface salinity decreases from 31 for present-day runoff to below 26 for a doubling of runoff. The freshening effect penetrates to the upper halocline (around 80 m), below which the salinity response is small. As the surface freshens, the upper ocean becomes more stratified, resulting in a shallower winter ML (lower dashed gray line in Figure 6a). Because the summer ML is always quite shallow due to shortwave heating and ice melt, the seasonal cycle in mixed layer depth (MLD) weakens (distance between the dashed gray lines in Figure 6a). Experiments with less river runoff than present-day feature a saltier, deeper ML with a larger seasonal cycle in depth. The full seasonal cycle of the temperature and density structure is shown in supporting information Figures S2 and S3.

The temperature response to increasing runoff can be seen in Figure 6b, with general warming extending through most of the Arctic column. The warming is strongest between 200 and 600 m, in the AW layer, but there is also significant warming just below the ML above the cold halocline (see also Figure 7). The structure of the temperature response is the result of an intricate adjustment in stratification and mixing as the surface ML freshens and thins. We examine the details of this adjustment in the next section.

To first order, the heat budget of the ML is a balance between the surface fluxes and entrainment from below. The simulated surface fluxes (Figure 8b) include longwave and shortwave radiation and turbulent heat fluxes over open ocean and sea ice, and their net effect is to cool the ML. The shortwave component (solar radiation input, simulated as an exponentially decaying function with depth) penetrates to depths of

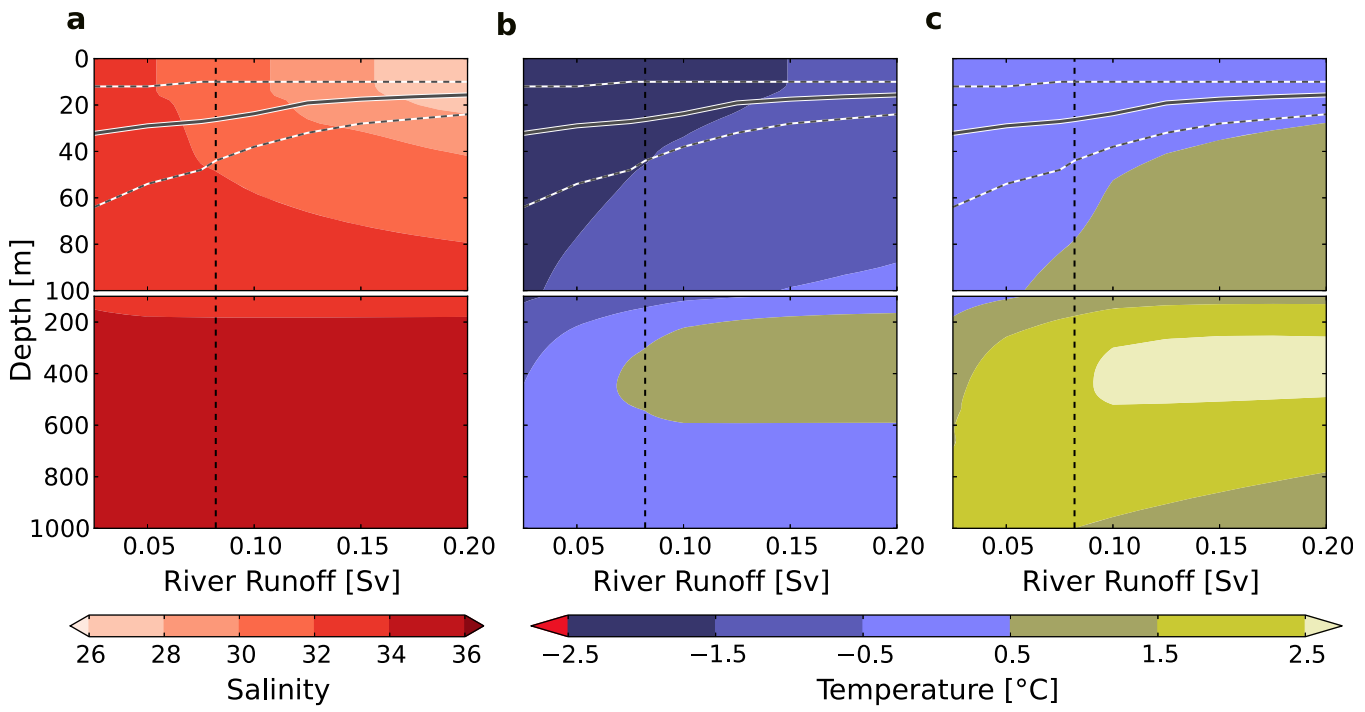

Figure 6. Simulated changes in (a) salinity (S), (b) temperature (T), and (c) temperature referenced to freezing point temperature (T_f) in response to increasing river runoff. The vertical black dashed line shows annual mean river runoff into the Arctic Ocean for the present day. The gray lines show the mixed layer depth (MLD; solid is annual mean, dashed are winter maximum and summer minimum).

60–70 m, so the influence of the surface fluxes also reaches these depths. The ML entrainment term (entrainment of water into the ML from below) consistently warms the ML (Figure 8c). At steady state, surface heat loss is compensated by entrainment of warmer waters through ML deepening. However, as increasing runoff causes the winter ML to shoal, a larger portion of the heat from shortwave radiation in summer is left in the water column in winter. This causes a warming of the upper halocline just below the winter ML, a feature similar to what is sometimes called the near-surface temperature maximum (NSTM) in observations [see also *Toole et al.*, 2010; *Jackson et al.*, 2011]. At lower runoffs, the winter ML forms deep enough that it reincorporates all the heat absorbed during summer.

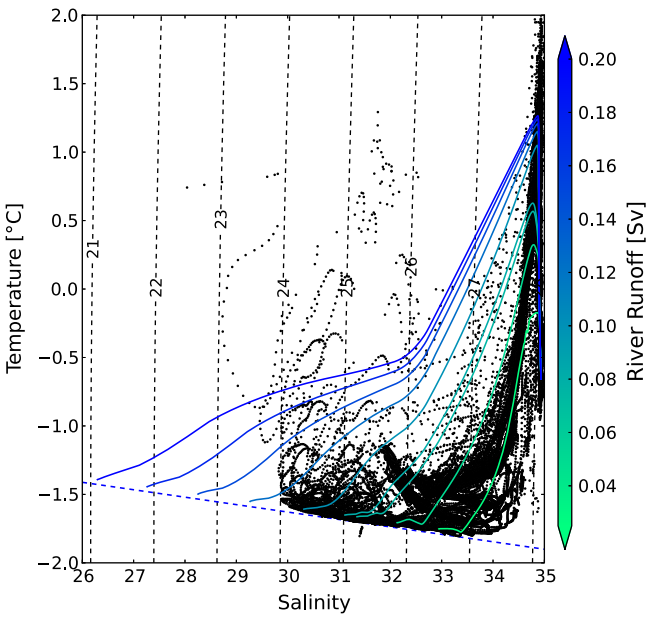

Figure 7. T-S diagram for the Arctic. The solid lines show the simulated steady state result for the runoff experiments, with colors indicating the runoff value. The black dots show observed climatological conditions (PHC3.0 updated from *Steele et al.* [2001]). The freezing point temperature is indicated by the dashed blue line.

The compensating heat flux in the AW layer warms nearly the entire column (Figure 8a). Recall that we fix the AW inflow properties in our experiments, so there is no change in T_{AW} and S_{AW} with time. The compensating heat flux balances the surface fluxes and maintains the warm subsurface waters for entrainment. The formulation of the interactive AW layer in 1DICEx carefully adjusts the implied AW volume flux to maintain this compensating heat flux. As runoff increases, the

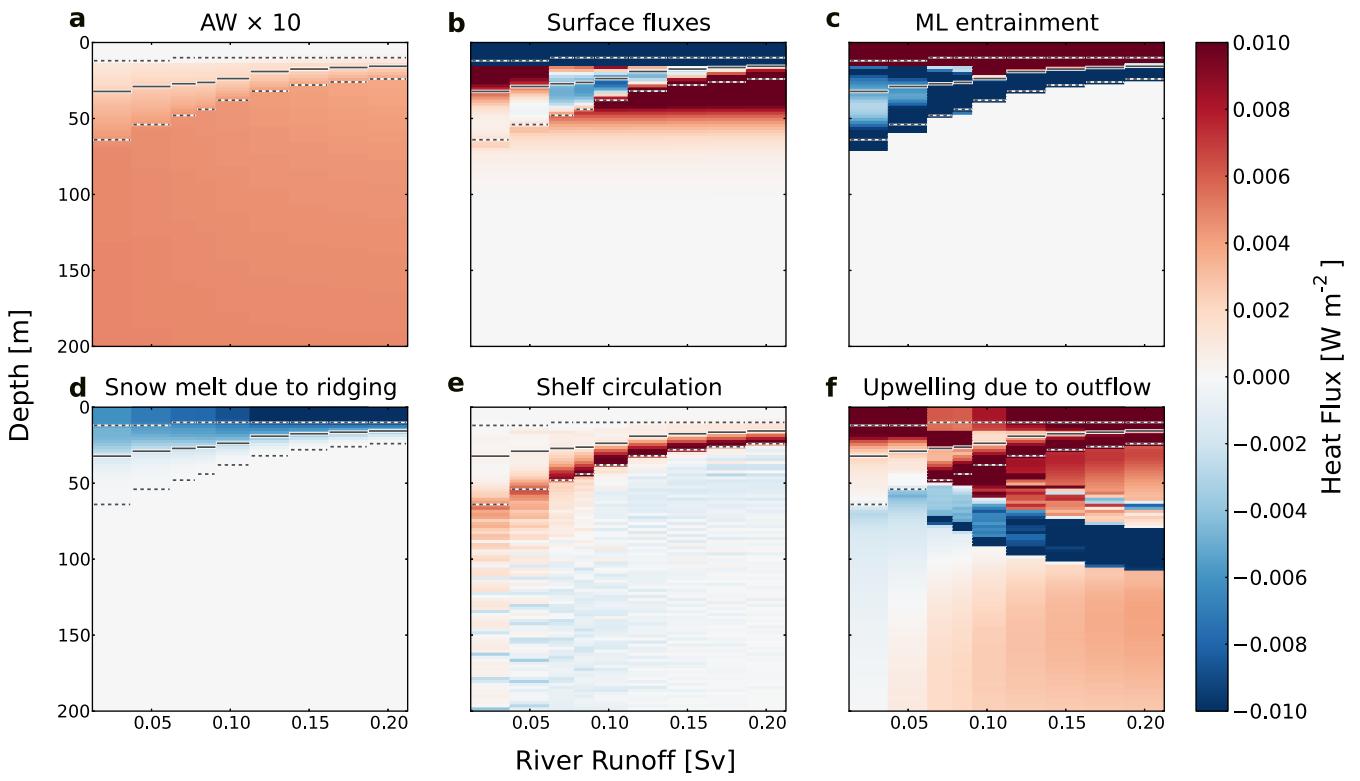

Figure 8. Contributions to heat flux convergence at each model level from: (a) compensating heat flux in the AW layer, (b) surface fluxes, (c) mixed layer entrainment, (d) snowmelt due to ridging, (e) shelf circulation, and (f) upwelling to replace geostrophic outflow. Note that the AW layer contribution is scaled by a factor of 10. The gray lines show the mixed layer depth (MLD; solid is annual mean, dashed are winter maximum and summer minimum).

stronger stratification inhibits entrainment, and more heat accumulates within the warming Atlantic layer (Figures 6b and 7). However, in equilibrium the warmer AW layer results in an increased vertical temperature gradient and vertical heat flux, balancing the compensating heat flux in AW layer. This mechanism is further discussed in the next section.

There are a number of additional terms that are important for closing the ocean heat budget. These also respond to changing runoff, but to a lesser degree. The snowmelt term (Figure 8d) comes from the sea ice ridging parameterization. When ridging occurs, the sea ice area fraction decreases, and the snow on the disappearing ice area is tipped into the ocean. The snowmelts in the ML, cooling it down. The shelf circulation term (Figure 8e) generally cools the waters below the ML and warms the lower part of the ML. Shelf water is created (parameterized) from ML water that enters the shelf area, cools to the freezing point, and becomes saltier due to brine rejection when sea ice forms. For mass continuity, the water leaving the ML and entering the shelf is replaced by warmer subsurface waters, a process that creates the warming signal seen at the base of the ML. The ML water modified on the shelf is injected into the halocline. Because this shelf water is at the freezing point, it has a cooling effect. Finally, upwelling due to geostrophic outflow from the column (Figure 8f) generally warms the upper water column because temperature increases with depth below the ML. However, because neither the temperature gradient nor the outflow are constant with depth, certain layers lose more heat upward than they receive from below, resulting in some localized cooling. It is worth noting that the geostrophic outflow increases as a function of the runoff leading to increased upwelling.

3.2. Sea Ice Response

Overall, the equilibrium changes in sea ice thickness with increasing runoff are small, on order of 15 cm (∼5%) at most (Figure 10). Increasing runoff leads to a decrease in surface salinity and increase in the vertical density gradient between the surface ML and the underlying AW layer. The stronger density gradient inhibits mixing of warm water to the surface (reduces vertical heat flux to the ML), which leads to warming of the column below the ML. At the same time, the subsurface warming increases the temperature gradient

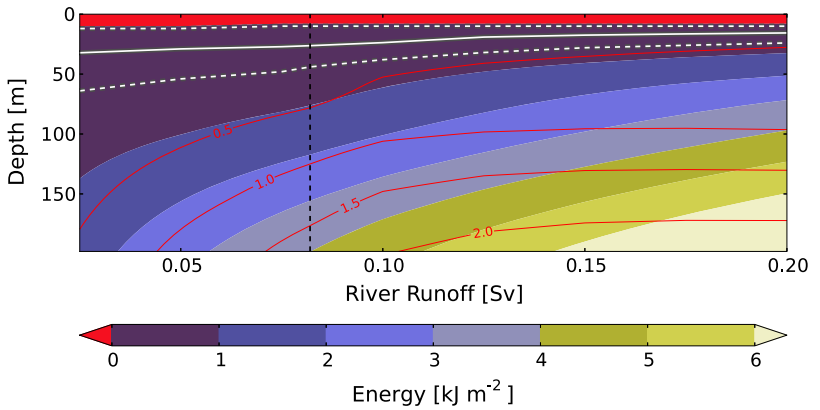

Figure 9. Energy required to mix away stratification as a function of river runoff. Color shading shows the energy (kJ m^{-2}) required to lift water from a given level to the surface mixed layer. Red contours show the temperature (°C) relative to the freezing point. The vertical black dashed line shows annual mean river runoff into the Arctic Ocean for the present day and the gray lines show the mixed layer depth (MLD; solid is annual mean, dashed are winter maximum and summer minimum).

between the ML and the underlying AW layer, making any mixing that does occur more effective (enhances vertical heat flux to the ML). The subsurface warming is a transient response that continues until the density and temperature gradients have adjusted to produce a vertical heat flux to the ML that is once again in equilibrium with the compensating heat flux below the ML.

One way to illustrate the net effect of the vertical temperature and density gradients is to calculate the mechanical energy needed to lift a parcel through the halocline to the ML. This represents the work done against gravity and is shown as a function of runoff in Figure 9. Just below the ML, the temperature contours follow remarkably well the energy contours. This implies that the energy needed to bring water of a certain temperature to the surface is largely independent of river runoff. Below 70–80 m and at runoffs above 0.1 Sv, the temperature contours become increasingly perpendicular to the energy contours. This suggests a more important role for runoff in the deep ocean, but note that mixing is parameterized with a constant diffusion coefficient in this part of the column.

While the balance of gradients accounts for why the steady state response of ice thickness to runoff is small, we must look to other factors to explain the subtle changes that do occur. In addition to the vertical heat flux from the ocean to the surface (or base of the ice), ice thickness also depends on the freezing point temperature T_f. Because freezing point temperature increases with the decreasing surface salinity, it is easier to form ice when there is more runoff, all other forcings remaining constant. A simple experiment shows that ice thickness can differ by a factor of two depending on whether constant or variable T_f is used (Figure 10). At runoff values larger than present day, about half (7 cm) of the ice thickening can be attributed to the effect of increasing T_f. SW radiation can also affect the column heat budget below the ML, as discussed in section 3.1. With present-day runoff, the heat from SW radiation that penetrates the ML is mixed back up during the next winter when the ML deepens. With more runoff, some of the SW heat remains trapped below the ML, further facilitating ice growth.

Increasing runoff alters the ice thickness distribution only slightly (not shown). The area of open water and the thinnest ice classes as well as that of the thickest ice classes appear to be largely unaffected. Most of the change in annual mean thickness (Figure 10a) comes from multiyear ice classes of 1–5 m thickness. This reflects the fact that ocean thermodynamical changes are most important for the nonridged multiyear ice classes while the thinnest and thickest ice classes are controlled by atmosphere and ice dynamics, respectively.

Finally, we note that our results include a slight imbalance in the ocean heat content that could be responsible for part of the ice thickness response to runoff. The column is not in complete equilibrium by the end of the 500 year simulations for the lower runoff scenarios (Figure 4). The immediate implication is that the assumptions of constant vertical heat flux discussed at the beginning of this section is not true for all scenarios, and varying ocean heat content could affect ice thickness as well.

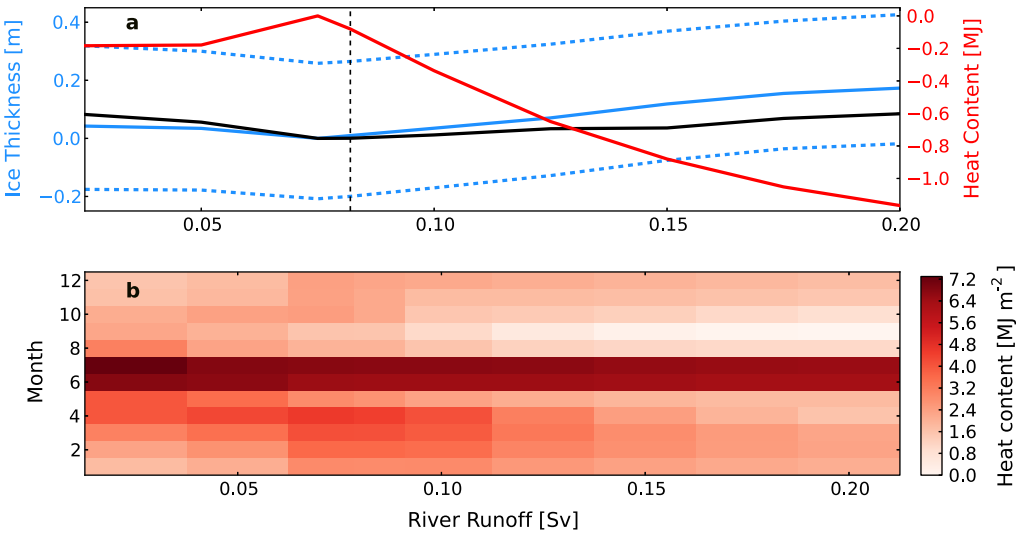

Figure 10. Simulated changes in sea ice thickness and mixed layer (ML) heat content in response to increasing river runoff. (a) The solid blue line is annual mean sea ice thickness calculated from the 42 model ice classes; the dashed blue lines are the seasonal maximum and minimum sea ice thickness; the solid black line is the same as solid blue line but for constant freezing point temperature. The red line is the annual mean ML heat content anomaly compared to case with 0.075 Sv runoff and when temperature is referenced to the surface freezing point. The vertical dashed black line shows annual mean river runoff into the Arctic Ocean for the present day. (b) Monthly climatology of ML heat content (relative to the freezing point temperature) as a function of river runoff.

4. Discussion

Our sensitivity study tests the response of an idealized Arctic Ocean to future increases in runoff, but some of the simulated results are consistent with observed changes in the Arctic under ongoing global warming. For example, warming of the AW layer has been observed, although the cause has been attributed to horizontal advection rather than changes in vertical stratification [*Schauer and Beszczynska-Möller*, 2009; *Grotefendt et al*., 1998]. Also storage of solar heating below the shallow ML has recently been documented in the Canadian basin [*Toole et al*., 2010; *Jackson et al*., 2011].

In addition, our results agree with previous analytical and simplified modeling studies. *Nilsson and Walin* [2010] found a shallower MLD and *Rudels* [2010] found increasing Arctic freshwater content as freshwater forcing increases. This is not surprising given that both studies are built on estuarine assumptions similar to ours, where the geostrophic outflow is balanced by vertical entrainment from the AW layer to the surface [*Stigebrandt*, 1981]. More recently, *Spall* [2013] developed an analytical model based on idealized, high resolution (eddy resolving) simulations of the Arctic Ocean. Here, the horizontal eddy transports from the boundary toward the interior are balanced by vertical entrainment in the interior, which is different from the estuarine model. Despite a different theoretical basis and conceptual model (see his Figure 11), the results are consistent with the ones presented here—that decreasing salinity at the boundary (as would be caused by increasing river runoff) leads to a thinner halocline and increased freshwater content in the Arctic domain.

While our study agrees rather well with other simplified modeling studies, the comparison to more complex model results is not as straightforward. For example, results from the 1DICEx model imply that a stronger density gradient across Fram Strait would lead to increased Fram Strait outflow by geostrophic arguments. However, *Arzel et al*. [2008] found a rapid decline in Fram Strait volume outflow in 20th and 21st century simulations performed with a coupled global climate model. They attributed decreased outflow to an atmospheric high pressure anomaly in the North Atlantic associated with surface freshening and sea ice expansion, a mechanism that is not represented in 1DICEx.

Assuming fixed North Atlantic temperature (T_{AW}) and salinity (S_{AW}) allows for a clean cause and effect study, but carries certain implications. Recall that the geostrophic surface outflow in 1DICEx is determined by the density difference between the North Atlantic (defined by T_{AW} and S_{AW}) and the Arctic column (prognostic). The assumption of fixed AW properties is reasonable for a system where freshwater outflow is small

compared to the volume of the surface layer in the North Atlantic. However, one might expect the AW properties—especially S_{AW}—to change as the Arctic comes to a long-term adjustment with increased runoff. Allowing the AW properties to vary would in some sense be more realistic, but it would also prevent us from identifying the isolated response to runoff.

In our perturbation experiments, all the forcings (including runoff) have a fixed seasonal cycle. In a warming climate, we might expect winter runoff to increase considerably but peak runoffs in late spring and summer to increase only a little if at all. Changes in ice growth and shelf water production would also be expected to be largest in winter, when these processes are most active. More runoff and a fresher surface could lead to shelf waters that are fresher and consequently less dense. While we have not accounted for these effects, they would likely affect any future change in the upper halocline of the Arctic Ocean.

One of the most poorly constrained parameters in our model is the vertical diffusion coefficient (κ). We chose κ along with T_{AW} and S_{AW} based on the available direct observations (section 2.2), and such that the set of values produced the best match to the observed T-S structure of the central Arctic Ocean. As with S_{AW}, it is likely that the value of κ varies with time. This variability could be driven by changes in the sea ice cover, which in turn alters the available fetch and size of waves produced during summer, the energy available for internal wave generation, and the associated mixing due to wave breaking. Given that the mean background level of vertical mixing in the Arctic Ocean is based on very few direct measurements [*Fer*, 2009; *Lique et al*., 2014] and is highly uncertain, a better observational basis is needed before we can reasonably introduce more complexity to how it is represented in the model.

Future work will focus on using more complex ocean and climate models to explore the regional expressions of the changes we have documented. NorESM future warming scenarios show similar Arctic responses to our 1DICEx study, with surface freshening, a sharpening of the halocline, and warming below the ML. In the NorESM scenarios, it is not only runoff that is changing, but preliminary runoff experiments with a stand-alone ocean-sea ice model also show similar results. Together, this range of modeling tools will help assess the regional variability and overall importance of the mechanisms presented here in a warming world.

5. Concluding Remarks

This study has investigated the response of a coupled atmosphere-ice-ocean column model of the Arctic Ocean to increasing river runoff. The column model reproduces the observed temperature and salinity structure of the central Arctic reasonably well. Increasing runoff freshens the surface and intensifies the stratification as expected, but also sharpens the halocline, and allows for larger heat content in the Atlantic Water layer with little change in the equilibrium vertical heat flux toward the surface. The equilibrium response of the 1DICEx column model to an increase in river runoff can be understood as follows.

1. Surface freshening leads to a stronger vertical density gradient, reduced mixing across the base of the ML, and a thinning of the ML. This tends to reduce the vertical heat flux toward the surface, thereby warming the AW layer.
2. A warmer AW layer leads to a stronger vertical temperature gradient across the halocline between the ML and the AW layer, which tends to enhance the vertical heat flux toward the surface.

The Arctic column reaches equilibrium when the vertical heat flux to the ML balances the compensating heat flux convergence in the AW layer. At equilibrium, changes in the net vertical heat flux in response to varying runoff are small.

1. Because the net vertical heat flux is not very sensitive to runoff, not much change is observed in either the heat supplied from the ocean to the base of the ice or the sea ice cover.
2. A modest increase in sea ice thickness (about 15 cm or 5%) is attributable to (1) an increase in the freezing point temperature of the ML as it freshens, and (2) an increase in the absorbed summer heat that is trapped below the ML and inaccessible to melt sea ice the following winter as the ML thins.

To better evaluate the effects of increased runoff (or any perturbation in stratification) to the Arctic in the future, tighter observational constraints on the large-scale vertical diffusion within the Arctic basin are needed.

Appendix A: Model Description

We review the most relevant parts of the model physics and describe the changes made for this study. The aim is to present the dynamical implications of the changes. For a complete description of the model development, the reader is referred to the studies by *Björk* [1989, 1992, 1997] and *Björk and Söderkvist* [2002]. See Appendix B for a table of the variable names and definitions and Appendix C for the climatological forcing used in this study.

A1. Ocean Component

The ocean model consists of a surface ML and the interior ocean. The bottom of the original model domain was set at 300 m, assumed to be the core of the Atlantic Water (AW) layer and also the level of no motion. We extend the bottom of the domain down to 2000 m and include a 500 m thick interactive AW layer that can respond to changes in river runoff.

In our extended model, the level of no motion is set to the depth of the temperature maximum in the column, which represents the core of the AW. This is an equivalent assumption to the original setup, where the level of no motion at the bottom of the domain (300 m) was also taken to represent the core of the AW and was set to a fixed AW temperature. To compensate the surface heat loss, we apply a constant heating term to the AW layer. This allows the temperature of the AW layer to adjust to runoff changes in the extended model. Note that the net heat transport into the column will not be constant because the overall balance is affected by adjustments in surface outflow, ice export (which represents heat transport into the column), and net surface radiation.

A1.1. Ocean Mixed Layer Dynamics

The ML dynamics are described in *Björk* [1989, 1997] and follow the pycnocline model developed by *Stigebrandt* [1985] [see also *Stigebrandt*, 1981], with conservation equations for ML thickness, temperature, and salinity.

The thickness of the ML, h, follows from the conservation of Arctic Ocean volume

$$\frac{dh}{dt}=(\mu Q_b+Q_f+\varepsilon Q_i+Q_g')\frac{1}{A}+w_e \tag{A1}$$

where μQ_b is the Bering Strait inflow (forcing), Q_f is the river runoff (forcing), ε is the fraction of ice to water density, ϵQ_i is the water equivalent of the net change in ice volume, Q_g' is the geostrophic outflow, w_e is the entrainment velocity representing mixing through the bottom of the ML, and A is the area of the Arctic basin (excluding the Barents Sea). All transports are defined to be positive when adding volume to the Arctic. The parameter μ is zero if Bering Strait water is denser than water in the ML, otherwise (normally) it is one.

The entrainment velocity is defined as

$$w_e=\frac{2m_0u_*^3/h_w-kB}{g'}=\frac{2m_0u_*^3/h_w-kB}{g(\rho(h)-\rho_m)/\rho(h)} \tag{A2}$$

where m_0 is a constant relating the Richardson flux number R_f and the ice-ocean drag coefficient C_{di} ($m_0=R_f/\sqrt{C_{di}}$), u^* is the friction velocity, h_w is the ML thickness excluding the ice thickness ($h_w=h-\varepsilon hi_i$), k is a factor controlling the energy available for mixing from the buoyancy flux B (0.05 when B is negative and 1 otherwise), g' is the reduced gravity, and ρ_m and $\rho(h)$ are the densities in and just below the ML, respectively.

The friction velocity, u^*, is a function of the ice velocity, Vi:

$$u_*^2=C_{di}Vi^2 \tag{A3}$$

The ice velocity is parameterized as a function of 10 m wind, W_{10} (forcing):

$$Vi=a_0W_{10} \tag{A4}$$

where a_0 is the ratio of wind speed to ice speed. *Linders and Björk* [2013] used the same model with an additional correction for W_{10} taking into account shorter term variability, but we do not adopt this correction.

The buoyancy flux B through the sea surface is defined as

$$B=g\left(\frac{\alpha Q_0}{c_{pw}\rho_w}-\beta(\varepsilon P_i S_m-Si+\varepsilon_s P_s S_m)+\frac{Q_f(\beta S_m+\alpha(T_m-T_r))}{A}+\frac{\mu Q_b(\beta(S_m-S_b)+\alpha(T_m-T_b))}{A}\right) \tag{A5}$$

where α is the thermal expansion coefficient, Q_0 is the net ice-ocean heat flux (mean over all ice classes, with positive values denoting a heat loss from the ocean), c_{pw} is the specific heat capacity of water, ρ_w is the density of water, β is the saline contraction coefficient, P_i is net ice growth, P_s is net snow accumulation, S_m is the salinity of the ML, Si is the salinity of the ice, T_r is the temperature of river water, and S_b and T_b are the specified salinity and temperature of the Bering Strait inflow. Positive values of B lead to positive w_e and deepening of the ML; if the Bering Strait water is denser than the model surface water then $\frac{Q_b(\beta(S_m-S_b)+\alpha(T_m-T_b))}{A}$ is zero. Negative values of B lead to negative w_e and thinning of the ML. For the thinning case, the thickness of the ML is set to the shorter of the Ekman (h_e) or Monin-Obukhov (h_m) lengths, defined as

$$h_e=\frac{Ku_*}{f} \tag{A6}$$

$$h_m=\frac{2m_0u_*}{B} \tag{A7}$$

where f is the Coriolis parameter and K is an empirical constant estimated to be 0.2 [*Björk*, 1989].

The ocean outflow Q'_g is parameterized assuming a geostrophically balanced coastal current following *Stigebrandt* [1981]. In this approach, the outflow at each level is the integral of the thermal wind equation from the bottom of the model domain to that level. The total outflow is the integral over the entire model domain multiplied by a scaling parameter λ, which depends on the number of outlets [*Björk*, 1989]. The outflow Q_T at each level i is

$$Q_T^i=\sum_{i=0}^{z}q^i\Delta z=\sum_{i=0}^{z}\left(-\frac{g}{\rho_{AW}f}\sum_{i=z}^{H_m}(\rho_{AW}-\rho^i)\Delta z\right)\Delta z \tag{A8}$$

where q^i is the geostrophic velocity at level i, ρ_{AW} is the AW density, and H_m is the level at which $\rho^i=\rho_{AW}$, i.e., the level of no motion. The total outflow from the basin is then given by

$$Q'_g=\lambda Q_T(i=h) \tag{A9}$$

In the model, the outflow is balanced by upwelling from the abyss, which means that the vertical velocity w_a at level i can be written as

$$w_a^i=\begin{cases}(\lambda Q_T^i+Q_f+\varepsilon Q_i)/A & i\le i_b\\(\lambda Q_T^i+Q_f+\varepsilon Q_i+Q_b)/A & i>i_b\end{cases} \tag{A10}$$

where i_b is the level where Bering Strait inflow is inserted.

A1.2. Ocean Mixed Layer Salt and Heat Balance

The salt balance for the ML is

$$\frac{dS_m}{dt}=\frac{(\mu Q_b(S_b-S_m)-Q_fS_m)/A+\varepsilon P_i(S_m-Si)+w_e(S_h-S_m)}{h_w} \tag{A11}$$

where S_h is the salinity just below the ML.

The ML temperature is calculated based on prognostic equations. As explained by *Björk* [1997], for heat conservation, different equations must be used during melting and freezing. The equations are shown below and the reader is referred to *Björk* [1997] for more details. The ML temperature change ΔT_m in a time step Δt is defined as

$$\Delta T_m = \left(\frac{F_w \Delta t}{\rho_w c_{pw}} + (T_f - T_m)\Delta H_w\right) \frac{1}{h_w + \Delta h_w}, \text{for melting} \tag{A12}$$

$$\Delta T_m = \frac{F_w \Delta t}{\rho_w c_{pw}(h_w + \Delta h_w)}, \text{for freezing} \tag{A13}$$

where ΔH_w is the thickness of the layer of water that is formed by melting of ice or that freezes.

A1.3. Interior Ocean and the Extended Domain

The rate of change below the ML at each level *i* for salinity and temperature is

$$\frac{dS^i}{dt} = w_a^i \frac{\partial S^i}{\partial z} + \kappa \frac{\partial^2 S^i}{\partial z^2} + \mu_2 F^i (S_{AW} - S^i) \tag{A14}$$

$$\frac{dT^i}{dt} = w_a^i \frac{\partial T^i}{\partial z} + \kappa \frac{\partial^2 T^i}{\partial z^2} + \mu_2 F^i (T_{AW} - T^i) \tag{A15}$$

The first terms in each equation $\left(w_a^i \frac{\partial S^i}{\partial z}$ and $w_a^i \frac{\partial T^i}{\partial z}\right)$ represent changes due to dynamical upwelling, and the second terms $\left(\kappa \frac{\partial^2 S^i}{\partial z^2}$ and $\kappa \frac{\partial^2 T^i}{\partial z^2}\right)$ represent changes due to background mixing set by the diffusion coefficient κ (see also the discussion in *Björk* [1989] about the numerical diffusion). For this study, κ is set to be 10% smaller below the Atlantic layer than in the rest of the column as very little mixing is assumed to occur in the deep ocean. The third terms ($\mu_2 F^i (S_{AW} - S^i)$ and $\mu_2 F^i (T_{AW} - T^i)$) represent the heat and salt supply to the AW layer required to compensate the surface forcing and outflow. (Physically, they represent the heat and salt supply by the AW inflow to the column.) μ_2 is a step function, defined to be 1 for the AW layer (a 500 m thick layer below the base of the ML) and 0 elsewhere; F^i is a time-varying parameter that depends on the heat content difference between the AW and the column (see below); and S_{AW} and T_{AW} are the prescribed AW temperature and salinity. These terms are not found in the original model, where the AW layer was set to constant temperature and salinity.

The AW inflow must compensate the surface forcing and outflow, and the prescribed value of AW heat transport is chosen to satisfy this. The main idea behind the formulation of the third terms in equations (14) and (15) is to bring in enough AW to meet the heat transport requirement. At each time step, a fraction Δh of each model level within the AW layer of the column is replaced by AW. This fraction is determined by dividing the prescribed AW heat transport in a time step (ΔQ_{AW}^i) by the difference in heat content between the AW and model level (ΔQ^i). The exact value of ΔQ_{AW}^i depends on how the total AW heat transport is partitioned among the various levels of the AW layer. At each vertical level *i* within the AW layer, we have

$$\Delta h_{AW}^i = \frac{\Delta Q_{AW}^i}{\Delta Q^i} \tag{A16}$$

We divide the equation by the time step Δt and expand the ΔQ^i term to arrive at the expression for F^i

$$F^i = \frac{\Delta h_{AW}^i}{\Delta t} = \frac{\Delta Q_{AW}^i / \Delta t}{Z_{AW} A c_{pw} (\rho_{AW} T_{AW} - \rho^i T^i)} \tag{A17}$$

where $H_{AW} = Q_{AW}^i / \Delta t$ is the AW heat transport in W m^{-2} (forcing), Z_{AW} is 500 m (thickness of the layer where parameterization is applied), c_{pw} is the specific heat of water (constant 4000 kg m^{-3} is assumed). ρ_{AW} and ρ^i are the AW and column densities, respectively.

Since Δh^i is physically a fraction of the layer thickness, we can calculate the total volume input Ψ associated with the AW heat input as

$$\Psi = \frac{A \cdot \Delta z}{\Delta t} \cdot \sum_i \Delta h^i \tag{A18}$$

where *i* goes from $Z/\Delta z$ levels below the ML to the bottom of the ML.

It is interesting to note that the formulation of the new terms $F^i (S_{AW} - S^i)$ and $F^i (T_{AW} - T^i)$ is numerically equivalent to nudging temperature and salinity toward AW values with a relaxation parameter F^i, although the physical reasoning is quite different. These terms have to do with the thermal component of the circulation, the part of the AW transport that is required for heat balance.

A1.4. Shelf Water Circulation

Ice growth on the shallow shelves is important for the formation of the Arctic halocline. 1DICEx includes this phenomenon through a parameterization in which ML water is assumed to flow to the shelf, where it mixes with brine created during the formation of sea ice. The resulting "shelf water" is close to freezing point temperature and is more saline than the original ML water. This cold, salty water mass is inserted into the column below the ML at the appropriate density. The most important equations are described below; more details can be found in *Björk* [1989, 1997].

The strength of the shelf water input into the column is a linear decreasing function of the salinity (S)

$$q_s = q_0 \frac{S_2 - S}{S_2 - S_m} \tag{A19}$$

where S_2 is the maximum salinity allowed for shelf water; S_m is the ML salinity and also the minimum salinity allowed for shelf water ($S_m \leq S \leq S_2$); and q_0 is the volume flux when $S = S_m$. The total volume flux Q_s and the total salt flux Θ from the shelf into the column are integrals over the salinity range:

$$Q_S = \int_{S_m}^{S_2} q_s dS = q_0 \frac{S_2 - S_m}{2} \tag{A20}$$

$$\Theta = \int_{S_m}^{S_2} q_s S dS = \frac{1}{6} q_0 (S_2 - S_m)(S_2 + 2S_m) \tag{A21}$$

For salt conservation, the inflow of salt from the shelf into the column Θ must be balanced by the outflow of salt from the ML to the shelf as well as ice formation. We can write

$$\Theta = Q_S S_m + \varepsilon Q_i (S_m - S_i) \tag{A22}$$

where $Q_i = p_s wiA$ is the ice volume export from the column, p_s denotes the fraction of total ice formation that contributes to shelf water production, wi is the ice growth velocity $\left(\frac{dhi}{dt}\right)$, and Si is the salinity of ice. By substituting (20) and (21) into (22), solving for q_0 and inserting this expression back into (20), we arrive at an expression for the total volume flux from the shelves as a function of ice formation (note that this flux only exists when ice is growing)

$$Q_S = \begin{cases} 3\varepsilon Q_i \dfrac{S_m - S_i}{S_2 - S_m} & Q_i > 0 \\ 0 & Q_i \leq 0 \end{cases} \tag{A23}$$

A2. Sea Ice Component

The sea ice component was described by [*Björk*, 1992, 1997]. We are using the same setup, and so give only a short review for reference. For clarity, we use the same notation as [*Björk*, 1992].

The basis of the ice model is a limited number of ice classes (C), each with an associated ice thickness (hi), snow thickness (hs), area (a), and internal temperature (Ti). For a given ice class i we can write

$$C_i = (a_i, hi_i, hs_i, Ti_i) \tag{A24}$$

where $i = 0, n$, and C_0 is the open water fraction and C_n the thickest ice. By definition, the sum of the fractional areas over all ice categories equals unity

$$\sum_{i=0}^{n} a_i = 1 \tag{A25}$$

The cumulative ice thickness distribution, $G(hi_i)$, is given by

$$G(hi_i) = \sum_{j=0}^{i} a_j \tag{A26}$$

The spatial mean ice thickness, $\langle hi \rangle$, is defined as

$$\langle hi \rangle = \sum_{i=0}^{n} hi_i \cdot a_i \tag{A27}$$

The quantities (a_i, hi_i, hs_i, Ti_i) of each ice class evolve over time. Dynamical processes affect a_i as they can create new ice classes by ridging and ice export. In addition, existing ice classes are merged if their thicknesses become similar enough. The thermodynamic part of the ice model affects hi_i, hs_i, and Ti_i through ice growth and melt within each ice class, which might also result in merging of ice classes. For computational efficiency, the number of ice classes is limited to 42, which is sufficient to simulate the Arctic ice thickness distribution. In the following, we review the formulation of the dynamic and thermodynamic ice processes in the model.

A2.1. Sea Ice Dynamics

The model dynamics include ridging and ice export, both of which affect the evolution of the fractional area (a_i) per ice class (i)

$$\frac{da_i}{dt} = E_i + R_i \tag{A28}$$

where Ei_i is the rate of change due to ice export out of the domain and R_i is the rate of change due to ridging for each ice class. Ice export is assumed to occur for all ice classes (excluding open water) and is parameterized as a function of area fraction of ice exported per unit time (ei_i). Export decreases the area fraction of all the ice classes and creates open water area fraction at the same rate. We can write

$$Ei_i = \begin{cases} ei_i & i=0 \\ -\dfrac{ei_i \cdot a_i}{1-a_0} & i=1,n \end{cases} \tag{A29}$$

where $i = 0$ denotes open water. If no open water is present, the model will always create a new $i = 0$ class at that time step.

The rate of deformation in each ice class due to ridging R_i is given by

$$R_i = \begin{cases} r_i & i=0 \\ -(r_i Ma_i)/((M-1)G_j) & i=1,j \\ 0 & i=j+1,n \\ (r_i a_{i-n})/((M-1)G_j) & i=n+1,n+j \end{cases} \tag{A30}$$

where r_i is the ridging area fraction change per unit time; M is the factor by which the ridging process thickens the ice. Note that the model differentiates between the deformed (ridged) and undeformed ice classes, creating new, ridged ice classes C_{n+1} to C_{n+j}. A cumulative fraction $G*$ determines the cutoff thickness (class $i = j$) above which ice is not ridged (in other words, the thinnest $G*$ fraction is active in the ridging process). After ridging, the model merges the new ridged ice classes with existing ice classes if their thicknesses are close enough. Snow thickness remains constant after ridging and the excess snow is given to the ML, where it is assumed to melt and alter the ML temperature and salinity.

The merging procedure is rather straightforward for the a_i, hi, and hs variables as they are simply area-weighted averages of the merging ice classes. Heat conservation requires a somewhat complicated calculation of the internal ice temperature [*Björk*, 1992]. During the summer melting season, the thinnest ice classes can also melt completely, in which case their area fraction merges with the open water class.

A2.2. Sea Ice Thermodynamics

The thermodynamic model is a simple, 1-level model where the ice has one internal temperature. Snow on top of the ice acts as an insulating layer. The model also includes internal phase changes and the effect of brine pockets inside the ice. The heat balance at the ice/snow surface is described in section A3 and the heat balance at the ocean/ice interface is described in section A1.

A3. Atmospheric Component

The atmosphere used in this model is a so-called "gray atmosphere," which is transparent to solar radiation [*Björk and Söderkvist*, 2002; *Thorndike and Colony*, 1982]. Because our study concentrates on the ice and

ocean components of the model, we review the atmospheric component briefly and refer the reader to *Björk and Söderkvist* [2002] for details. The vertical coordinate of the model atmosphere is the optical height, a length measure of absorbance in the longwave spectrum. The total optical depth is the optical height at the top of the atmosphere. A balance can be found between the upward and downward thermal radiation and the atmospheric heat transport at each optical height. The main interest in terms of the paper is the coupling at the surface where the upward conductive heat flux through the ice and snow is balanced by the net radiative and turbulent heat fluxes at the surface. The surface heat balance is thus given by

$$C_c(T_s - Ti) = (1-\alpha_s)F_{sw} + F_{DN}(0) - (A_{SB} + B_{SB}T_s) + C_T(T_a(0) - T_s) \tag{A31}$$

where $C_c(T_s - Ti)$ is the conductive heat flux from the ice/snow to the surface, C_c is a coefficient depending on the conductivity and thickness of the ice and snow layers, T_s is the surface temperature, Ti is the internal ice temperature, α_s is the surface albedo, F_{sw} is the incoming shortwave radiation (forcing), $F_DN(0)$ is the downward longwave radiation at the lowest atmospheric level, $A_{SB} + B_{SB}T_s$ is the Stefan-Boltzmann law linearized around the freezing point, and the $C_T(T_a(0) - T_s)$ term represents the turbulent heat flux from the surface.

Because there are multiple ice categories with different ice thicknesses, snow thicknesses and internal temperatures, the above heat balance must be satisfied for each category. The surface temperature for each ice class i is written:

$$T_s^i = \frac{(1-\alpha^i)F_{sw} - A_{SB} + C_c^i T^i + F_{DN}(0) + C_T T_a(0)}{B_{SB} + C_T + C_C^i} \tag{A32}$$

The atmosphere feels the area-averaged surface temperature over all the ice classes.

Appendix B: List of Symbols

The list of symbols and their definitions are given in Table B1.

Table B1. List of Symbols and Their Definitions[a]

Symbol	Definition	Variable Type	Value if Constant
α	Thermal expansion coefficient	Prognostic	
α_s	Surface albedo	Prognostic	
A	Area of the Arctic Ocean	Constant	0.7×10^{13} m^2
A_{SB}	Constant in the linearized Stefan-Boltzmann law	Constant	320 W m^{-2}
a	Ice category area fraction (0–1)	Prognostic	
a_0	Wind-ice speed ration	Constant	0.01
β	Haline contraction coefficient	Prognostic	
B	The buoyancy flux through the sea surface	Prognostic	
B_{SB}	Coefficient in the linearized Stefan-Boltzmann law	Constant	4.6 W m^{-2}
C_{di}	Ice-ocean drag coefficient	Constant	5.5×10^{-3}
C	Ice category		
C_c	Ice conductivity coefficient	Constant	2.034 W m K^{-1}
c_p	Specific heat of sea water	Constant	4.0 kJ kg K^{-1}
c_{pw}	Specific heat of water	Constant	4.18 kJ kg K^{-1}
C_T	Turbulent heat exchange coefficient at the surface	Constant	1.75×10^{-3}
ϵ	Ratio between the ice and water density	Constant	0.9
Ei	Rate of ice area fraction change due to ice export	Prognostic	
ei	Ice export in unit time	Prognostic	
f	Coriolis parameter	Constant	1.43×10^{-4} s^{-1}
F^i	Ocean relaxation parameter	Prognostic	
F_{DN}	Atmospheric downward longwave radiation	Forcing	
F_{SW}	Surface shortwave radiation	Prognostic	
g'	Reduced gravity	Prognostic	
g	Gravitational acceleration coefficient	Constant	9.81 m s^{-2}
G	Cumulative thickness distribution	Prognostic	
G_*	Ridging cutoff value for cumulative ice area fraction	Constant	7%
Δh^i	Fraction of the ocean level	Prognostic	
ΔH_w	Thickness of melted or frozen ice as water	Prognostic	
H_{AW}	Atlantic heat transport	Constant	1 TW
$\langle H \rangle$	Area-weighted mean ice thickness	Prognostic	
h	Ocean mixed layer thickness	Prognostic	
h_e	Ekman length scale	Prognostic	
hi	Ice thickness	Prognostic	

Table B1. (continued)

Symbol	Definition	Variable Type	Value if Constant
h_m	Monin-Obukhov length scale	Prognostic	
hs	Snow thickness	Prognostic	
h_w	Ocean mixed layer thickness excluding ice thickness	Prognostic	
κ	Internal mixing coefficient in the ocean	Constant	4.0 m^2 s^{-1}
λ	Scaling parameter for ocean outflows	Constant	0.7
μ	Bering Strait outflow flag	Constant	1 or 0
μ_2	AW inflow flag	Constant	1 or 0
M	Ridge thickness multiplier	Constant	6
m_0	$R_f/\sqrt{C_{di}}$	Constant	0.674
P_i	Net ice growth/melt	Prognostic	
P_s	Net snow accumulation/melt	Prognostic	
q	Geostrophic velocity at each level	Prognostic	
q_s	Volume flux toward the shelf	Prognostic	
q_0	Volume flux toward the shelf when the $S = S_m$	Prognostic	
ΔQ_{AW}	Atlantic heat transport in a time steps	Constant	
Q_0	Net ice-ocean heat flux	Prognostic	
Q_b	Bering Strait volume inflow	Forcing	
Q_f	River runoff	Forcing	
Q_i	Ice volume export	Prognostic	
Q'_g	Geostrophic outflow	Prognostic	
Q_S	Total volume flux due to shelf water production	Prognostic	
Q_T	Thermal wind transport	Prognostic	
ρ	Density of the ocean column	Prognostic	
ρ_{AW}	Density of the Atlantic inflow	Constant	1027.8 kg m^{-3}
ρi	Density of ice	Constant	900 kg m^{-3}
ρ_w	Density of water	Constant	1000 kg m^{-3}
R_f	Flux Rickhardson number	Constant	0.05
R	Rate of ice area fraction change due to ridging	Prognostic	
S	Salinity of the ocean column	Prognostic	
S_b	Bering Strait inflow salinity	Forcing	
S_{AW}	Salinity of the Atlantic inflow	Constant	35 g kg^{-1}
S_m	Mixed layer salinity	Prognostic	
Si	Salinity of the ice	Constant	5 g kg^{-1}
S_2	Maximum salinity of the shelf water	Constant	34.8 g kg^{-1}
S_h	Salinity just below the mixed layer	Prognostic	
T	Temperature of the ocean column	Prognostic	
T_a	Atmospheric temperature	Prognostic	
T_{AW}	Temperature of the Atlantic inflow	Constant	3.5°C
T_b	Bering Strait inflow temperature	Forcing	
T_f	Freezing point temperature	Prognostic	
Ti	(Internal) ice temperature	Prognostic	
T_m	Mixed layer temperature	Prognostic	
T_r	River water temperature	Constant	0°C
T_s	Surface temperature	Prognostic	
Θ	Total salt flux due to shelf water production	Prognostic	
u^*	Ocean friction velocity	Prognostic	
Vi	Ice velocity	Prognostic	
Z	Extent of the Atlantic heat transport	Constant	500 m
w_a	Upwelling velocity in the ocean column	Prognostic	
w_e	Entrainment velocity to the mixed layer	Prognostic	
wi	Ice growth velocity	Prognostic	
W_{10}	10 m wind velocity	Forcing	
Ψ	Total volume input by the AW parameterization	Prognostic	

[a]Variable types as follows: constant for model parameters, forcing for constants with seasonal cycle, prognostic for all model variables that are computed for new every time step.

Appendix C: Model Forcing

The climatological forcing used in this study is given in Table C1. Note that the river runoff is scaled from the climatological values so that the annual mean runoff is increased by the desired amount.

Table C1. Climatological Forcing Following *Björk and Söderkvist* [2002]

Variable	January	February	March	April	May	June	July	August	September	October	November	December
Surface SW radiation (W m^{-2})	0.0	5.1	32.9	142.4	256.8	302.0	232.6	132.9	47.6	9.6	0.0	0.0
Atm. heat transport (W m^{-2})	127.0	109.8	119.7	106.2	72.6	78.4	87.8	88.4	93.5	108.1	121.4	122.7

Table C1. (continued)

Variable	January	February	March	April	May	June	July	August	September	October	November	December
Optical thickness	2.3	2.3	2.3	2.3	4.5	5.3	5.3	5.3	5.3	4.5	3.1	2.3
Relative humidity	0.85	0.85	0.88	0.88	0.89	0.93	0.93	0.94	0.88	0.85	0.85	0.85
Snow albedo	0.85	0.84	0.83	0.81	0.82	0.78	0.64	0.69	0.84	0.85	0.85	0.85
Snow accumulation (mm d^{-1})	0.83	0.83	0.83	0.83	5.00	0.00	0.00	0.00	12.87	12.87	0.83	0.83
10 m wind velocity (m s^{-1})	5.6	5.7	5.3	5.1	5.0	5.2	5.2	5.4	6.2	6.2	5.8	5.5
Wind velocity std (m s^{-1})	3.3	3.3	3.0	3.0	2.7	2.9	3.1	3.2	3.8	3.5	3.5	3.2
Ice/wind velocity ratio (%)	1	1	1	1	1	2	2	2	1	1	1	1
Wind stress (N m^{-2})	5	5	5	5	5	5	5	5	5	5	5	5
River runoff (Sv)	0.026	0.021	0.022	0.023	0.106	0.294	0.164	0.117	0.094	0.063	0.031	0.026
Bering Strait inflow (Sv)	1.02	0.95	0.34	0.78	1.13	1.26	1.47	1.07	0.66	0.87	0.90	0.34
Bering Strait inflow S	32.2	32.6	32.7	32.6	32.3	32.2	32.4	32.1	32.0	31.6	31.5	31.7
Bering Strait inflow T (°C)	−1.7	−1.8	−1.8	−1.8	−1.2	0.8	3.8	4.3	4.2	3.1	−1.2	−1.7

Acknowledgments

This work was supported by the Bjerknes Centre project DYNAWARM. C.L. acknowledges the support of the Centre for Climate Dynamics (SKD) at the Bjerknes Centre. Thanks to Mehmet Ilicak, Doug Martinson, Bob Newton, Peter Schlosser, Bruno Tremblay, and Ingrid Onarheim for stimulating discussions and helpful suggestions on the manuscript. We also thank the three anonymous reviewers for their constructive comments on the manuscript. All the data, the model setup, and the analyzing scripts used in this study are available through the corresponding author by email at aleksi.nummelin@gfi.uib.no.

References

Arzel, O., T. Fichefet, H. Goosse, and J.-L. Dufresne (2008), Causes and impacts of changes in the Arctic freshwater budget during the twentieth and twenty-first centuries in an AOGCM, *Clim. Dyn.*, *30*(1), 37–58, doi:10.1007/s00382-007-0258-5.

Bentsen, M., et al. (2013), The Norwegian Earth System Model, NorESM1-M. Part 1: Description and basic evaluation of the physical climate, *Geosci. Model Dev.*, *6*(3), 687–720, doi:10.5194/gmd-6-687-2013.

Björk, G. (1989), A one-dimensional time-dependent model for the vertical stratification of the upper Arctic Ocean, *J. Phys. Oceanogr.*, *19*, 52–67, doi:10.1175/1520-0485(1989)019<0052:AODTDM>2.0.CO;2.

Björk, G. (1992), On the response of the equilibrium thickness distribution of sea ice to ice export, mechanical deformation, and thermal forcing with application to the Arctic Ocean, *J. Geophys. Res.*, *97*(C7), 11,287–11,298, doi:10.1029/92JC00814.

Björk, G. (1997), The relation between ice deformation, oceanic heat flux, and the ice thickness distribution in the Arctic Ocean, *J. Geophys. Res.*, *102*(C8), 18,681–18,698, doi:10.1029/97JC00789.

Björk, G., and J. Söderkvist (2002), Dependence of the Arctic Ocean ice thickness distribution on the poleward energy flux in the atmosphere, *J. Geophys. Res.*, *107*(C10), 3173, doi:10.1029/2000JC000723.

Dunne, J. P., et al. (2012), GFDLs ESM2 global coupled climate-carbon earth system models. Part I: Physical formulation and baseline simulation characteristics, *J. Clim.*, *25*(19), 6646–6665, doi:10.1175/JCLI-D-11-00560.1.

Fer, I. (2009), Weak vertical diffusion allows maintenance of cold halocline in the central Arctic, *Atmos. Oceanic Sci. Lett.*, *2*(3), 148–152.

Grotefendt, K., K. Logemann, D. Quadfasel, and S. Ronski (1998), Is the Arctic Ocean warming?, *J. Geophys. Res.*, *103*(C12), 27,679–27,687, doi:10.1029/98JC02097.

Jackson, J. M., S. E. Allen, F. A. McLaughlin, R. A. Woodgate, and E. C. Carmack (2011), Changes to the near-surface waters in the Canada Basin, Arctic Ocean from 1993–2009: A basin in transition, *J. Geophys. Res.*, *116*, C10008, doi:10.1029/2011JC007069.

Jones, C. D., et al. (2011), The HadGEM2-ES implementation of CMIP5 centennial simulations, *Geosci. Model Dev.*, *4*(3), 543–570, doi:10.5194/gmd-4-543-2011.

Lammers, R. B., A. I. Shiklomanov, C. J. Vörösmarty, B. M. Fekete, and B. J. Peterson (2001), Assessment of contemporary Arctic river runoff based on observational discharge records, *J. Geophys. Res.*, *106*(D4), 3321–3334, doi:10.1029/2000JD900444.

Linders, J., and G. Björk (2013), The melt-freeze cycle of the Arctic Ocean ice cover and its dependence on ocean stratification, *J. Geophys. Res. Oceans*, *118*, 5963–5976, doi:10.1002/jgrc.20409.

Lique, C., J. D. Guthrie, M. Steele, A. Proshutinsky, J. H. Morison, and R. Krishfield (2014), Diffusive vertical heat flux in the Canada Basin of the Arctic Ocean inferred from moored instruments, *J. Geophys. Res. Oceans*, *119*, 496–508, doi:10.1002/2013JC009346.

Marnela, M., B. Rudels, M.-N. Houssais, A. Beszczynska-Möller, and P. B. Eriksson (2013), Recirculation in the Fram Strait and transports of water in and north of the Fram Strait derived from CTD data, *Ocean Sci.*, *9*(3), 499–519, doi:10.5194/os-9-499-2013.

Mignot, J., D. Swingedouw, J. Deshayes, O. Marti, C. Talandier, R. Séférian, M. Lengaigne, and G. Madec (2013), On the evolution of the oceanic component of the IPSL climate models from CMIP3 to CMIP5: A mean state comparison, *Ocean Modell.*, *72*, 167–184, doi:10.1016/j.ocemod.2013.09.001.

Nilsson, J., and G. Walin (2010), Salinity-dominated thermohaline circulation in sill basins: Can two stable equilibria exist?, *Tellus, Ser. A*, *62*(2), 123–133, doi:10.1111/j.1600-0870.2009.00428.x.

Overeem, I., and J. P. M. Syvitski (2010), Shifting discharge peaks in Arctic rivers, 1977–2007, *Geogr. Ann., Ser. A*, *92*(2), 285–296, doi:10.1111/j.1468-0459.2010.00395.x.

Peterson, B. J., R. M. Holmes, J. W. McClelland, C. J. Vörösmarty, R. B. Lammers, A. I. Shiklomanov, I. A. Shiklomanov, and S. Rahmstorf (2002), Increasing river discharge to the Arctic Ocean, *Science*, *298*(5601), 2171–2173, doi:10.1126/science.1077445.

Rawlins, M. A., et al. (2010), Analysis of the Arctic system for freshwater cycle intensification: Observations and expectations, *J. Clim.*, *23*(21), 5715–5737, doi:10.1175/2010JCLI3421.1.

Rudels, B. (2010), Constraints on exchanges in the Arctic Mediterranean-do they exist and can they be of use?, *Tellus, Ser. A*, *62*(2), 109–122, doi:10.1111/j.1600-0870.2009.00425.x.

Rudels, B., E. P. Jones, L. G. Anderson, and G. Kattner (1994), On the intermediate depth waters of the Arctic Ocean, in *The Polar Oceans and Their Role in Shaping the Global Environment*, edited by O. M. Johannessen, R. D. Muench, and J. E. Overland, AGU, Washington, D. C., doi:10.1029/GM085p0033.

Rudels, B., L. G. Anderson, and E. P. Jones (1996), Formation and evolution of the surface mixed layer and halocline of the Arctic Ocean, *J. Geophys. Res.*, *101*(C4), 8807–8821, doi:10.1029/96JC00143.

Rudels, B., E. P. Jones, U. Schauer, and P. B. Eriksson (2004), Atlantic sources of the Arctic Ocean surface and halocline waters, *Polar Res.*, *23*(2), 181–208, doi:10.1111/j.1751-8369.2004.tb00007.x.

Schauer, U., and A. Beszczynska-Möller (2009), Problems with estimation and interpretation of oceanic heat transport conceptual remarks for the case of Fram Strait in the Arctic Ocean, *Ocean Sci.*, *5*(4), 487–494, doi:10.5194/os-5-487-2009.

Smedsrud, L. H., A. Sorteberg, and K. Kloster (2008), Recent and future changes of the Arctic sea-ice cover, *Geophys. Res. Lett.*, *35*, L20503, doi:10.1029/2008GL034813.

Spall, M. A. (2013), On the circulation of Atlantic Water in the Arctic Ocean, *J. Phys. Oceanogr.*, *43*(11), 2352–2371, doi:10.1175/JPO-D-13-079.1.

Spreen, G., S. Kern, D. Stammer, and E. Hansen (2009), Fram Strait sea ice volume export estimated between 2003 and 2008 from satellite data, *Geophys. Res. Lett.*, *36*, L19502, doi:10.1029/2009GL039591.

Steele, M., and T. J. Boyd (1998), Retreat of the cold halocline layer in the Arctic Ocean, *J. Geophys. Res.*, *103*(C5), 10,419–10,435, doi:10.1029/98JC00580.

Steele, M., R. Morley, and W. Ermold (2001), PHC: A global ocean hydrography with a high-quality Arctic Ocean, *J. Clim.*, *14*(9), 2079–2087, doi:10.1175/1520-0442(2001)014<2079:PAGOHW>2.0.CO;2.

Stigebrandt, A. (1981), A model for the thickness and salinity of the upper layer in the Arctic Ocean and the relationship between the ice thickness and some external parameters, *J. Phys. Oceanogr.*, *11*(10), 1407–1422, doi:10.1175/1520-0485(1981)011<1407:AMFTTA>2.0.CO;2.

Stigebrandt, A. (1985), A model for the seasonal pycnocline in rotating systems with application to the Baltic proper, *J. Phys. Oceanogr.*, *15*, 1392–1404, doi:10.1175/1520-0485(1985)015<1392:AMFTSP>2.0.CO;2.

Thorndike, A. S., and R. Colony (1982), Sea ice motion in response to geostrophic winds, *J. Geophys. Res.*, *87*(C8), 5845–5852, doi:10.1029/JC087iC08p05845.

Toole, J. M., M.-L. Timmermans, D. K. Perovich, R. A. Krishfield, A. Proshutinsky, and J. A. Richter-Menge (2010), Influences of the ocean surface mixed layer and thermohaline stratification on Arctic Sea ice in the central Canada Basin, *J. Geophys. Res.*, *115*, C10018, doi:10.1029/2009JC005660.

Vinje, T. (2001), Fram Strait ice fluxes and atmospheric circulation: 1950–2000, *J. Clim.*, *14*, 3508–3517, doi:10.1175/1520-0442(2001)014<3508:FSIFAA>2.0.CO;2.